

1 **Title: Plasmodesmal connectivity in C₄ *Gynandropsis gynandra* is induced by light**
2 **and dependent on photosynthesis**

3
4
5 **Authors:**

6 Tina B. Schreier^{1,*}, Karin H. Müller², Simona Eicke³, Christine Faulkner⁴, Samuel C.
7 Zeeman³ and Julian M. Hibberd^{1,*}

8
9 **Affiliations:**

10 ¹ Department of Plant Sciences, University of Cambridge, Downing Street, CB1 3EA
11 Cambridge, United Kingdom

12 ² Cambridge Advanced Imaging Centre (CAIC), University of Cambridge, Downing Street,
13 CB2 3DY Cambridge, United Kingdom

14 ³ Institute of Molecular Plant Biology, ETH Zurich, CH-8092 Zurich, Switzerland

15 ⁴ Cell and Developmental Biology, John Innes Centre, Norwich Research Park, Norwich
16 NR4 7UH, United Kingdom

17
18 * Correspondence: tbs32@cam.ac.uk, jmh65@cam.ac.uk

19
20
21 **Running title: Light-induced plasmodesmata formation**

22
23 **Keywords:** Plasmodesmata, photosynthesis, C₄ photosynthesis, light,
24 photomorphogenesis, bundle sheath, mesophyll

25
26
27 **SUMMARY (200 words)**

28 **INTRODUCTION (722 words)**

29 **MATERIALS AND METHODS (1304 words)**

30 **RESULTS (1831 words)**

31 **Figures 1-6, all Figures should be published in colour**

32 **Supporting information: Figures 1-5, Videos 1-3.**

33 **DISCUSSION (1315 words)**

34
35 **Total (5379 words)**

36 **SUMMARY**

- 37
- 38 • In leaves of C₄ plants the reactions of photosynthesis become restricted between two
39 compartments. Typically, this allows accumulation of C₄ acids in mesophyll cells to
40 drive their diffusion into the bundle sheath. In C₄ monocotyledonous grasses
41 proliferation of plasmodesmata between these cell types is thought to increase cell-
42 to-cell connectivity to allow efficient metabolite movement. However, it is not clear if
43 C₄ dicotyledons also show enhanced plasmodesmal connectivity between these cell
44 types and whether this is a general requirement for C₄ photosynthesis is not known.
45 How mesophyll and bundle sheath cells in C₄ leaves become highly connected is
46 also not known.
 - 47 • We investigated these questions using 3D- and 2D- electron microscopy on the C₄
48 dicotyledon *Gynandropsis gynandra*, and phylogenetically close C₃ relatives.
 - 49 • The mesophyll-bundle sheath interface of C₄ *G. gynandra* showed higher
50 plasmodesmal frequency compared with closely related C₃ species. Formation of
51 these plasmodesmata was induced by light. Pharmacological agents that perturbed
52 chloroplast development or photosynthesis reduced the number of plasmodesmata,
53 but this inhibitory effect could be reversed by the provision of exogenous sucrose.
 - 54 • We conclude that the enhanced plasmodesmata formation between mesophyll and
55 bundle sheath cells of C₄ *G. gynandra* appears to be wired to the induction of C₄
56 photosynthesis.
57
58
59

60 INTRODUCTION

61 C₄ photosynthesis represents a carbon concentration mechanism that evolved
62 independently over 60 times from the ancestral C₃-type of photosynthesis (Sage et al.
63 (2011)). In leaves of C₄ plants, HCO₃⁻ is initially fixed by Phosphoenolpyruvate Carboxylase
64 (PEPC) in mesophyll (M) cells into a 4-carbon acid (malate/aspartate), which is transferred
65 to bundle sheath (BS) cells for decarboxylation to produce pyruvate and CO₂. Pyruvate is
66 transferred back to the mesophyll cells, where it is reduced to phosphoenolpyruvate that can
67 accept another CO₂ molecule. This spatial separation of carboxylation and decarboxylation
68 between mesophyll and bundle sheath cells builds a high concentration of CO₂ in bundle
69 sheath cells and in so doing limits the oxygenation side reaction of RuBisCO (Hatch, 1987).
70 This greatly increases photosynthesis efficiency, particularly in hot and dry environments.

71 An efficient exchange of metabolites between mesophyll and bundle sheath cells is
72 therefore crucial to the C₄ pathway and as a consequence compared with the ancestral C₃
73 condition C₄ leaves are typically reconfiguration in terms of both biochemical pathways and
74 anatomy. Most C₄ plants have Kranz anatomy - with closely spaced veins and a wreath-like,
75 concentric arrangement of enlarged bundle sheath cells that are directly adjacent to
76 mesophyll cells, maximizing mesophyll-bundle sheath contact sites (Sedelnikova et al.,
77 2018). Kranz anatomy is associated with increased cell-to-cell connectivity between the
78 mesophyll and bundle sheath cells to allow the efficient exchange of metabolites. Metabolite
79 exchange between the two cell types is proposed to occur via passive diffusion through
80 plasmodesmata, down a steep concentration gradient of C₄ metabolites (Hatch, 1987).
81 Plasmodesmata are regulated channels between adjacent plant cells and diverse in
82 structure: from simple (with single openings in adjacent cells) to complex (highly branched
83 with central cavities), or even asymmetric in their organisation (Ross-Elliott et al., 2017;
84 Faulkner, 2018). Plasmodesmata contain several structural components including a narrow
85 tube of endoplasmic reticulum called the desmotubule, the cytoplasmic sleeve and the
86 plasma membrane (Faulkner, 2018). Plasmodesmata are considered essential for cell-to-
87 cell transport of metabolites in many C₄ grasses because suberized bundle sheath cell walls
88 likely reduce CO₂ leakage by blocking apoplastic metabolite transfer (Hatch and Osmond,
89 1976). Furthermore, C₄ grasses possess increased numbers of plasmodesmata at the
90 mesophyll – bundle sheath cell interface (Evert et al., 1977; Botha et al., 1992; Danila et al.,
91 2016). As plasmodesmata occur in clusters (pitfields), increased cell-to-cell connectivity in
92 C₄ leaves can be a result of increased pit field area or increased numbers of plasmodesmata
93 per pit field area. Danila et al. (2016) observed up to 9-fold increase in plasmodesmal
94 frequency at the mesophyll-bundle sheath interface in C₄ maize and *Setaria viridis*

95 compared with the C₃ species rice and wheat. This increase in the C₄ grasses was due to a
96 2-fold increase in plasmodesmata numbers per pitfield, and a 5-fold increase in pitfield area.
97 In other C₄ grass species substantial variation in absolute plasmodesmata frequency was
98 evident but they all possessed greater plasmodesmata frequency than C₃ species (Danila
99 et al., 2018).

100 To our knowledge, the distribution of plasmodesmata at the mesophyll-bundle sheath cell
101 interface between C₃ and C₄ species has not been studied outside the grasses. Further, the
102 cues that underpin increased plasmodesmata formation are not known. Given the known
103 variation in how increased cell-to-cell connectivity is achieved in C₄ grasses and the fact that
104 they evolved C₄ photosynthesis independently from C₄ dicotyledenous lineages, we
105 assessed plasmodesmata distribution in leaves of C₃ *Tarenaya hassleriana* and C₄
106 *Gynandropsis gynandra* that both belong to the *Cleomaceae* (Brown et al., 2005; Marshall
107 et al., 2007) which is sister to the *Brassicaceae*. *G. gynandra* has been developed as a C₄
108 model (Brown et al., 2005; Marshall et al., 2007; Koteyeva et al., 2011). We discovered that
109 plasmodesmal frequency is up to 8-fold higher at the mesophyll-bundle sheath cell interface
110 in mature leaves of C₄ *G. gynandra* compared with that in C₃ species. Moreover, these
111 increased numbers of plasmodesmata are rapidly established during de-etiolation.
112 Pharmacological studies using multiple chloroplast inhibitors demonstrated that light,
113 functional chloroplasts and photosynthesis are required to initiate plasmodesmata formation
114 at mesophyll-bundle sheath cell interface of *G. gynandra*. Provision of exogenous sucrose
115 can rescue defects in chloroplasts and photosynthesis. We conclude that increased cell-to-
116 cell connectivity is likely an unifying feature of all two-celled C₄ plants, and that during the
117 evolution of the C₄ pathway the increased formation of secondary plasmodesmata is
118 induced by the induction of photosynthesis itself.

119

120 MATERIAL AND METHODS

121 Plant Material and growth conditions

122 *G. gynandra* and *T. hassleriana* seeds were germinated on wet filter papers in petri
123 dishes. For *G. gynandra*, germination was initiated by exposing seeds to 30°C for 24 h. For
124 *T. hassleriana*, germination was stimulated by an alternating temperature regime of 12 h
125 32°C then 12 h at 20°C for 5 consecutive days. After germination, *G. gynandra* and *T.*
126 *hassleriana* seedlings were planted in 10:1 ratio of M3 compost (Levington Advance, Pot
127 and Bedding, High Nutrient):fine vermiculite in individual pots. *A. thaliana* (Col-0) was sown
128 onto potting compost (Levington Advance, Solutions) with 0.17 g L⁻¹ insecticide (thiacloprid,
129 Exemptor) and stratified for 48 h at 4°C. Around 2 weeks after germination, individual
130 seedlings were transplanted to individual pots.

131 To sample of mature leaves, plants were grown in a climate-controlled growth chamber
132 with 16-h light and 8-h dark. *G. gynandra* and *T. hassleriana* were grown at 350 μmol
133 photons m⁻² s⁻¹ at 25°C with a 60% (v/v) relative humidity and ambient CO₂. *A. thaliana*
134 plants were grown under identical conditions except light intensity was 150 μmol photons
135 m⁻² s⁻¹. All plants were watered by an automated system whereby the bottom of the trays
136 was flooded to a depth of 4 cm every 48 h for 10 min, after which the irrigation water was
137 drained.

138 For deetiolation experiments, *G. gynandra* seeds were germinated with the addition of
139 0.15% (v/v) plant preservative mixture (Apollo Scientific, CAS: 26172-55-4) to the wet filter
140 paper. Germinated seedlings were transferred to square plates containing half-strength MS
141 (Murashige and Skoog) salts with B5 vitamins (Duchefa Biochemie BV) and 0.8% (w/v) agar
142 (Melford) in the dark. Plates were grown in the plant growth cabinet (Panasonic MLR-352
143 PE) at 20 °C with continuous light intensity of 150 μmol m⁻² s⁻¹. Plates were covered with
144 aluminum foil for three consecutive days to ensure no light was able to penetrate. Aluminum
145 foil was removed on day 3 and to allow de-etiolation plants grown for an additional 24 to 48
146 h in the light. For sucrose supplementation, 10 g L⁻¹ sucrose was added to the half-strength
147 MS media. For inhibitor treatments, 500 μM lincomycin (Sigma Aldrich), 50 μM norflurazon
148 (Sigma Aldrich) and 20 μM DCMU (Sigma Aldrich) were added to the half-strength MS
149 media before the media was poured in the individual petri dishes. As norflurazon and
150 lincomycin were dissolved in ethanol, the control and DCMU treatments included an
151 equivalent amount of ethanol in the media.

152

153

154

155 **Electron microscopy**

156 Samples from 5-8 individual seedlings at each time point were harvested for electron
157 microscopy. Leaf segments (~2 mm²) were excised with a razor blade and immediately fixed
158 in 2% (v/v) glutaraldehyde and 2% (w/v) formaldehyde in 0.05 - 0.1 M sodium cacodylate
159 (NaCac) buffer (pH 7.4) containing 2 mM calcium chloride. Samples were vacuum infiltrated
160 overnight, washed 5 times in 0.05 – 0.1 M NaCac buffer, and post-fixed in 1% (v/v) aqueous
161 osmium tetroxide, 1.5% (w/v) potassium ferricyanide in 0.05 M NaCac buffer for 3 days at
162 4°C. After osmication, samples were washed 5 times in deionized water and post-fixed in
163 0.1% (w/v) thiocarbohydrazide for 20 min at room temperature in the dark. Samples were
164 then washed 5 times in deionized water and osmicated for a second time for 1 h in 2% (v/v)
165 aqueous osmium tetroxide at room temperature. Samples were washed 5 times in deionized
166 water and subsequently stained in 2% (w/v) uranyl acetate in 0.05 M maleate buffer (pH 5.5)
167 for 3 days at 4°C, and washed 5 times afterwards in deionized water. Samples were then
168 dehydrated in an ethanol series, transferred to acetone, and then to acetonitrile. Leaf
169 samples were embedded in Quetol 651 resin mix (TAAB Laboratories Equipment Ltd) and
170 cured at 60°C for 2 days.

171

172 **Transmission electron microscopy (TEM) and Scanning electron microscopy (SEM)**

173 For TEM, ultra-thin sections were cut with a diamond knife using a Leica Ultracut microtome
174 and collected on copper grids and examined in a FEI Tecnai G2 transmission electron
175 microscope (200 keV, 20 µm objective aperture). Images were obtained with an AMT CCD
176 camera. For SEM of plasmodesmata pitfields in *G. gynandra*, *T. hassleriana* and *A. thaliana*,
177 samples were prepared according to Danila et al. (2018). In summary, mature leaves were
178 cut into 10-20 mm strips and fixed in 2% (v/v) glutaraldehyde and 2% (w/v) formaldehyde in
179 0.05 - 0.1 M sodium cacodylate (NaCac) buffer (pH 7.4) containing 2 mM calcium chloride
180 under vacuum infiltration overnight at RT. Leaf tissue was dehydrated in an ethanol series
181 and critical point dried (CPD) in a Quorum E3100 dryer. CPD leaf samples were ripped apart
182 using forceps and sticky tape. Ripped samples were mounted on aluminum SEM stubs using
183 conductive carbon tabs (TAAB), sputter-coated with a thin layer of iridium (15 nm) and
184 imaged in a Verios 460 scanning electron microscope (FEI, Hillsboro, OR) run at an
185 accelerating voltage of 2 keV and 25 pA probe current. Low magnification images were
186 acquired with an Everhart-Thornley detector whilst high-resolution images were acquired
187 using the through-lens detector in immersion mode.

188 For 2D SEM mapping, ultra-thin sections were placed on Melinex (TAAB Laboratories
189 Equipment Ltd) plastic coverslips mounted on aluminum SEM stubs using conductive

190 carbon tabs (TAAB Laboratories Equipment Ltd), sputter-coated with a thin layer of carbon
191 (~ 30 nm) to avoid charging and imaged in a Verios 460 scanning electron microscope at 4
192 keV accelerating voltage and 0.2 nA probe current using the concentric backscatter detector
193 in field-free (low magnification) or immersion (high magnification) mode (working distance
194 3.5 – 4 mm, dwell time 3 μ s, 1536 x 1024 pixel resolution). For plasmodesmata frequency
195 quantification, SEM stitched maps were acquired at 10,000X magnification using the FEI
196 MAPS automated acquisition software. Greyscale contrast of the images were inverted to
197 allow easier visualisation.

198 Serial block face scanning electron microscopy (SBF-SEM) was performed on Quetol 651
199 resin-embedded mature leaf samples of *G. gynandra*, *T. hassleriana* and *A. thaliana* as
200 described above. Overviews of leaf cross-sections and the zoomed stacks of the mesophyll
201 – bundle sheath cell interface (\approx 300-400 images) were acquired through sequentially
202 sectioning the block faces at 50 nm increments and imaging the resulting block-face by
203 SEM. Images were acquired with a scanning electron microscope TFS Quanta 250 3VIEW
204 (FEI, Hillsboro, OR) at 1.8-2 keV with an integrated 3VIEW stage and a backscattered
205 electron detector (Gatan Inc., Pleasanton, CA, USA). Images were aligned and smoothed
206 using the plugins MultiStackReg and 3D median filter on ImageJ.

207 Plasmodesmal frequency from 2D and 3D EM images was determined using published
208 methods (Koteyeva et al., 2014; Botha, 1992). Briefly, plasmodesmal frequency was
209 determined as the number of plasmodesmata observed per μ m of length of shared cell
210 interface between two cell types (mesophyll – bundle sheath, mesophyll – mesophyll, bundle
211 sheath – bundle sheath). Plasmodesmata numbers and cell lengths were determined using
212 ImageJ software. Plasmodesmata were defined as dark channels in the EM images.
213 Depending on plasmodesmata orientation, the entire channel was sometimes not visible on
214 2D EM images, and so only channels that spanned more than half of the cell wall width were
215 counted.

216

217 **Chlorophyll fluorescence measurement**

218 Chlorophyll fluorescence measurements were carried out using a CF imager
219 (Technologica Ltd, UK) and image processing software provided by the manufacturer.
220 Seedlings were placed in the dark for 20 min evaluate dark-adapted minimum fluorescence
221 (F_0), dark-adapted maximum fluorescence (F_m) and then variable fluorescence F_v
222 ($F_v = F_m - F_0$). All chlorophyll fluorescence images of inhibitor-treated seedlings within each
223 experiment were acquired at the same time in a single image, measuring a total of 8
224 seedlings per treatment.

225

226 **Statistical analysis**

227 In violin plots, the middle line represents the median, the box and whiskers represent the
228 25 to 75 percentile and minimum-maximum distributions of the data. Letters show the
229 statistical ranking using a one-way ANOVA and post hoc Tukey test (different letters indicate
230 differences at $P < 0.05$). Values indicated by the same letter are not statistically different.
231 Data was analyzed using RStudio 2022.07.2+576.

232 **RESULTS**

233 **Plasmodesmata frequency is higher in C₄ *G. gynandra* leaves compared with C₃ *A.***
234 ***thaliana* and *T. hassleriana***

235 We first explored whether the increased plasmodesmal connectivity between mesophyll
236 and bundle sheath cells found in C₄ grasses was also present in the C₄ dicotyledon
237 *Gynandropsis gynandra*. Transmission electron microscopy was used to examine the
238 mesophyll-bundle sheath cell interface in mature leaves of *G. gynandra* plants and the
239 closely related C₃ species *Tarenaya hassleriana* (also a member of the *Cleomaceae*) and
240 C₃ model *Arabidopsis thaliana*. Plasmodesmata were more abundant at mesophyll-bundle
241 sheath interfaces in C₄ *G. gynandra* compared with both C₃ species (Fig. 1). The increased
242 physical connectivity was specific to this interface, and no obvious increases were detected
243 between the mesophyll-mesophyll or bundle sheath-bundle sheath cell interfaces in any of
244 the species (Supporting Information Fig. S1).

245 To quantify plasmodesmata numbers between mesophyll-bundle sheath cells, we
246 conducted serial block-face scanning electron microscopy (SBF-SEM). SBF-SEM offers
247 excellent resolution in 3D and has previously been used to quantify plasmodesmata in other
248 systems (Ross-Elliott et al., 2017; Paterlini and Belevich, 2022). Thin sections prepared from
249 fully expanded true leaves of *G. gynandra*, *T. hassleriana* and *A. thaliana* were imaged and
250 a mesophyll-bundle sheath cell interface area for serial block face sectioning was identified
251 (Fig. 2a-c). From each species, between 281-438 serial transverse sections per mesophyll-
252 bundle sheath cell interface were collected and compiled into videos (Supporting Information
253 Videos S1-3). Using these SBF-SEM sections we quantified plasmodesmata frequency by
254 determining the number of plasmodesmata per length of mesophyll-bundle sheath cell
255 interface imaged in 3D (Fig. 2d). In C₄ *G. gynandra*, plasmodesmata were visible in almost
256 every mesophyll-bundle sheath cell interface assessed such that only 20 out of 467
257 contained no plasmodesmata at all (Fig. 2d). In contrast, in the two C₃ species
258 plasmodesmata were not detected in the majority of interfaces (263/367 for *T. hassleriana*,
259 628/886 for *A. thaliana*). Because plasmodesmata appear in clusters (pitfields) rather than
260 being equally distributed, a wide range of plasmodesmal frequencies per section were
261 observed between mesophyll and bundle sheath cells in all three species. However, there
262 were more sections with higher frequencies observed at the mesophyll-bundle sheath
263 interface of C₄ *G. gynandra*, and this resulted in a 13-fold increase in the mean frequency
264 compared with C₃ *T. hassleriana* and C₃ *A. thaliana* (Fig. 2d). Plasmodesmal frequencies
265 between mesophyll and bundle sheath cells of the C₃ species *T. hassleriana* and *A. thaliana*
266 were not significantly different to each other and were low compared with C₄ *G. gynandra*.

267 SBF-SEM provides an excellent 3D view of plasmodesmata frequency and distribution
268 but is relatively low throughput and so limited numbers of cell interfaces can be visualised
269 per unit time. We therefore used 2D electron microscopy to further explore the high
270 occurrence of plasmodesmata at the mesophyll-bundle sheath cell interface of C₄ *G.*
271 *gynandra*. Large areas of leaf sections were imaged at high resolution using 2D Scanning
272 Electron Microscopy (SEM) mapping such that automated serial imaging at 10,000X
273 magnification and subsequent image stitching enabled visualization of plasmodesmata at
274 numerous interfaces within the same 2D section (Fig. **3a**). Representative SEM maps in
275 which cell interfaces (mesophyll-bundle sheath, mesophyll-mesophyll and bundle sheath-
276 bundle sheath) were pseudocoloured according to their plasmodesmal frequency, and
277 consistent with the 3D SBF-SEM analysis reported above, illustrated that plasmodesmata
278 were specifically enriched at the mesophyll-bundle sheath interface of C₄ *G. gynandra*
279 (indicated by the numerous green-coloured interfaces). In contrast, frequency was lower
280 and more uniform between all cellular interfaces in C₃ species (indicated by the pink and
281 orange pseudocoloured cell interfaces) (Fig. **3a**). Plasmodesmata frequencies were
282 quantified from at least three SEM maps originating from three independent plants
283 (biological replicates; 10-40 individual mesophyll – bundle sheath, mesophyll-mesophyll and
284 bundle sheath-bundle sheath cell interfaces per biological replicate). This showed that
285 plasmodesmata numbers between mesophyll and bundle sheath cells were more than 8-
286 fold higher in C₄ *G. gynandra* compared with both C₃ species. The three cellular interfaces
287 (mesophyll-bundle sheath, mesophyll-mesophyll and bundle sheath-bundle sheath) in both
288 C₃ species had similar plasmodesmal frequencies. Interestingly, plasmodesmal frequency
289 of all three types of cell interface in *G. gynandra* was significantly higher than that of the
290 corresponding interface in each of the two C₃ species. The mesophyll-mesophyll and bundle
291 sheath-bundle sheath interfaces were approximately 3-4-fold and 2-fold higher in C₄ *G.*
292 *gynandra* compared with *T. hassleriana* and *A. thaliana* respectively, indicating that cell-to-
293 cell connectivity is generally enhanced between photosynthetic cells of the C₄ species (Fig.
294 **2b**). Plasmodesmata frequencies estimated from analysis of numerous mesophyll-bundle
295 sheath cell interfaces using this 2D SEM mapping were not statistically different from the
296 frequencies obtained from multiple serial sections of the mesophyll-bundle sheath interface
297 using SBF-SEM (Supporting Information Fig. 2). To allow greater replication and sampling
298 subsequent analysis was therefore carried out with the 2D SEM mapping technique.

299 To investigate the relationship between increased frequency of plasmodesmata at the
300 mesophyll-bundle sheath interface and pit fields, we visualized pitfields using SEM by
301 tearing critical point dried mature leaves as described in Danila et al. (2016). Pitfields were

302 clearly visible at the mesophyll-bundle sheath interface in all species, but unlike the previous
303 work in grasses, individual plasmodesmata within the pitfields could not be distinguished
304 (Supporting Information Fig. **3a**). When we measured the mean area of pitfields in each
305 species there was no clear difference. This suggests that the increased plasmodesmata
306 frequency at mesophyll-bundle sheath in *G. gynandra* most likely results from increased pit
307 field numbers per cell interface rather than enlarged pit fields that contain more
308 plasmodesmata (Supporting Information Fig. **3b**).

309

310 **Increased plasmodesmal frequency between mesophyll and bundle sheath cells of** 311 **C₄ *G. gynandra* is established after exposure to light**

312 Induction of the photosynthetic apparatus associated with the C₄ pathway, such as
313 chloroplast development and C₄ gene expression typically occurs rapidly in response to light
314 (Shen et al., 2009; Singh et al., 2021). Such de-etiolation analysis is simplest if cotyledons
315 can be analysed, and as cotyledons of *G. gynandra* have C₄ anatomy (Koteyeva et al., 2011)
316 we examined plasmodesmata in cotyledons during de-etiolation. Cross sections of
317 cotyledons showed that Kranz anatomy was already partially developed in 3-day-old dark
318 grown seedlings (Fig. **4a**). For example, veins were closely spaced, and bundle sheath cells
319 contained abundant organelles. However, after 24 h of light cotyledons had almost doubled
320 in size and substantial cell expansion and formation of air spaces was evident (Fig. **4a**).
321 High-resolution 2D SEM maps from cross sections of at least three cotyledons (biological
322 replicates) of *G. gynandra* were obtained at 0 h, 24 h and 48 h after transfer to light.
323 Surprisingly, in dark-grown seedlings plasmodesmal frequency at mesophyll-bundle sheath,
324 mesophyll-mesophyll, and bundle sheath-bundle sheath were similar (n = 204) (Fig. **4c,d**).
325 However, after light induction plasmodesmal frequency increased 1.7-fold after 24 h and
326 2.5-fold after 48 h between mesophyll and bundle sheath cells of *G. gynandra* (Fig. **4b-d**).
327 There was also a small increase in plasmodesmata numbers between mesophyll and
328 mesophyll cells after light exposure. These responses were specific to de-etiolation because
329 growth in the dark for 48 h did not increase plasmodesmata numbers (Supporting
330 Information Fig. **4a-d**). These data indicate that as with true leaves, cotyledons of *G.*
331 *gynandra* develop high plasmodesmal connectivity between mesophyll and bundle sheath
332 cells, and that this takes place rapidly in response to light. We conclude that light is a crucial
333 developmental cue for the formation of secondary plasmodesmata at the mesophyll-bundle
334 sheath interface in the C₄ plant *G. gynandra*.

335

336 **Functional chloroplasts are required for light-induced formation of plasmodesmata**
337 **between the mesophyll and bundle sheath**

338 De-etiolation involves the transition from skotomorphogenic to photomorphogenic growth
339 whereby fully photosynthetic chloroplasts develop from etioplasts within hours of light
340 exposure (Pipitone et al., 2021; Singh et al., 2021; Cackett et al., 2021). Therefore, it is
341 possible that the increase in plasmodesmal connectivity at the mesophyll – bundle sheath
342 interface during de-etiolation is either a direct response to light or is triggered by signals
343 from the chloroplast or photosynthesis. To investigate this, we used inhibitors with distinct
344 modes of action to perturb chloroplast function. Lincomycin and norflurazon block plastid
345 translation and carotenoid biosynthesis respectively and so stop the development of
346 chloroplasts from etioplasts (Mulo et al., 2003; Chamovitz et al., 1991); Fig. **5b**). DCMU [3-
347 (3,4-dichlorophenyl)-1,1-dimethylurea] blocks the electron transport chain at Photosystem II
348 (PSII) (Trebst, 2007) and thus inhibits photosynthesis directly. Seedlings were grown with
349 and without each inhibitor and seedlings transferred to light for 48 h. Lincomycin- and
350 DCMU-treated seedlings had pale yellow cotyledons indistinguishable from non-treated
351 controls. Norflurazon treatment generated seedlings with white cotyledons, consistent with
352 compromised carotenoid accumulation (Fig. **5a**). Etioplast ultrastructure was largely
353 unaffected by the inhibitor treatments (Fig. **5b**). After 48 h of light, cotyledons of controls and
354 DCMU-treated seedlings were green and etioplasts had developed into chloroplasts (Fig.
355 **5a,b**). Norflurazon and lincomycin-treated seedlings had pale cotyledons even after light
356 induction and their etioplast-to-chloroplast development was arrested (Fig. **5a,b**). To confirm
357 that each inhibitor had the expected effect on chloroplast function we used chlorophyll
358 fluorescence imaging to quantify F_v/F_m which provides a read-out for the maximum quantum
359 efficiency of Photosystem II. Each of the inhibitors drastically reduced F_v/F_m compared with
360 controls (Fig. **5c,d**). Norflurazon-treated seedlings were not visible on the chlorophyll
361 fluorescence imager as chlorophyll content was too low.

362 Using 2D SEM maps we quantified plasmodesmal frequency by counting the number of
363 plasmodesmata and measuring the length of shared cell wall. This was conducted for nearly
364 1200 independent cell interfaces from each treatment (549 interfaces for the 0 h time point,
365 649 interfaces for the 48 h time point). None of the three inhibitors affected plasmodesmal
366 frequency at any cell interface in dark-grown seedlings (Fig. **5e-g**). However, despite
367 cotyledon expansion being unaffected by the inhibitors during de-etiolation (Supporting
368 Information Fig. **5a**) plasmodesmal frequencies did not increase significantly in seedlings
369 treated with norflurazon, lincomycin or DCMU (Fig. **5e-g**, Supporting Information Fig. **5b**). In
370 summary, inhibitors that perturbed the etioplast-to-chloroplast transition, or blocked

371 photosynthetic electron transport, reduced light-induced plasmodesmata formation at the
372 mesophyll-bundle sheath cell interface of C₄ *G. gynandra*. We conclude that chloroplast
373 function, and in particular photosynthetic electron transport, play an important role in
374 controlling the formation of secondary plasmodesmata in the C₄ leaf.

375 The inhibitory effect of DCMU on plasmodesmata formation could be associated with
376 signalling from a dysfunctional photosynthetic electron transport chain, or because less
377 photosynthate is produced. To test the latter hypothesis plants were grown on sucrose
378 during DCMU treatment. No distinguishable effects on phenotype of the seedlings or
379 etioplast-to-chloroplast development were detected (Fig. **6a,b**) and provision of sucrose did
380 not rescue the reduction in F_v/F_m caused by DCMU (Fig. **6c,d**). We quantified plasmodesmal
381 frequencies in a total of 1655 cell interfaces (mesophyll-bundle sheath, mesophyll-
382 mesophyll, bundle sheath-bundle sheath) among the different DCMU/sucrose treatments
383 (Fig. **6e-g**). Strikingly, DCMU-treated seedlings supplemented with sucrose had
384 plasmodesmal frequencies at the mesophyll-bundle sheath interface comparable to
385 untreated seedlings (Fig. **6e**, $p > 0.05$), indicating full rescue by sucrose of the DCMU-
386 induced inhibition of plasmodesmata formation (Fig. **6e**). Thus, when photosynthetic
387 electron transport is inhibited, sucrose is sufficient to restore plasmodesmata formation at
388 the mesophyll-bundle sheath cell interface.

389

390 **DISCUSSION**

391 **Increased plasmodesmata frequency is a conserved C₄ trait**

392 A critical feature of C₄ photosynthesis is the spatial separation of biochemical processes
393 such that CO₂ can be concentrated around RuBisCO. The consequence of this partitioning
394 of photosynthetic reactions is an absolute requirement for the exchange of metabolites
395 between cell types. In C₄ grasses this has long been associated with increased
396 plasmodesmal frequency between mesophyll and bundle sheath cells (Evert et al., 1977).
397 Despite the very different leaf morphology between monocotyledons and dicotyledons our
398 results reveal that increased plasmodesmal connectivity between mesophyll-bundle sheath
399 cells is likely a conserved trait among C₄ plants. Our findings are therefore consistent with
400 increased plasmodesmal connectivity representing a unifying trait of all C₄ species that
401 separate photosynthesis between two cell types. In *G. gynandra*, the mesophyll-bundle
402 sheath interfaces had 8-13-fold higher plasmodesmata frequency than those of the closely
403 related C₃ species *T. hassleriana* and *A. thaliana* (Fig. 1-3). This increase is comparable to
404 plasmodesmata numbers and distributions reported for C₄ grasses (Botha et al., 1992;
405 Danila et al., 2016). Danila et al. (2018) reported that C₄ grasses running the NAD-ME
406 subtype of C₄ photosynthesis had the highest numbers of plasmodesmata between
407 mesophyll and bundle sheath cells. As *G. gynandra* also primarily uses NAD-ME to
408 decarboxylate CO₂ in the bundle sheath, broader analysis of C₄ dicotyledons is required to
409 determine the extent to which plasmodesmal frequencies correlate with the various
410 biochemical sub-types.

411 Plasmodesmal frequencies at the mesophyll-bundle sheath interface of *G. gynandra* are
412 consistent with those reported previously in this species where no analysis of closely related
413 C₃ plants were possible (Koteyeva et al., 2014). By quantifying plasmodesmata at all
414 interface types and comparing plasmodesmal frequency with phylogenetically proximate C₃
415 plants we demonstrate that plasmodesmata numbers are generally higher at all three types
416 of cell interface (mesophyll-bundle sheath, mesophyll-mesophyll, bundle sheath-bundle
417 sheath) in C₄ *G. gynandra*. This is consistent with previous work that observed increased
418 plasmodesmata frequencies between photosynthetic leaf cells in C₄ grasses compared to
419 C₃ grasses (Danila et al., 2016).

420 A distinguishing feature of increased plasmodesmal frequency between the mesophyll
421 and bundle sheath cells of *G. gynandra* compared with C₄ grasses, is that the increase in
422 *G. gynandra* occurred without any detectable increase in pitfield area compared with C₃ *T.*
423 *hassleriana* and C₃ *A. thaliana* (Supporting Information Fig. 2). This suggests that the
424 primary mechanism for increased plasmodesmata numbers in *G. gynandra* is an increase

425 in pitfields. Since we were not able to visualise individual plasmodesmata within pitfields,
426 we cannot rule out that there is a higher frequency of individual plasmodesmata number
427 within pitfields in *G. gynandra*. However, this is unlikely since pitfield appearance was largely
428 similar between *G. gynandra*, *T. hassleriana* and *A. thaliana* (Supporting Information Fig. 2).
429 In contrast, increased plasmodesmal frequency in C₄ grasses was accompanied by
430 increases in pitfield area such that were up to 5 times greater than those in C₃ species
431 (Danila et al., 2016, 2018). This difference suggests that the mechanisms by which
432 increased plasmodesmata numbers between mesophyll and bundle sheath cells can vary
433 between C₄ lineages.

434 Flux of metabolites between cells is likely to be determined by plasmodesmata number
435 as increased numbers can facilitate greater flux. However, bundle sheath cells are not air-
436 tight and plasmodesmata could also contribute to CO₂ leakiness such that a proportion of
437 the CO₂ concentrated in the bundle sheath diffuses back to the mesophyll. CO₂ leakiness
438 particularly increases during photosynthetic induction in NADP-ME type C₄ plants such as
439 sorghum and maize (Wang et al., 2022). Thus, it is possible that plasmodesmata number
440 and distribution need to be optimised to allow maximum photosynthetic efficiency in C₄
441 plants. Being able to accurately quantify plasmodesmal traits in diverse C₄ species may be
442 crucial to develop further understanding in this area, and in particular in modelling metabolite
443 flux through the C₄ pathway (Danila et al., 2016; Von Caemmerer, 2021). These could
444 incorporate recent models of metabolite diffusion through plasmodesmata, such as the
445 geometric and narrow escape models (Denim et al., 2019; Hughes et al., 2021).

446

447 **Light triggers rapid plasmodesmata formation in mostly pre-existing cell walls**

448 In C₄ grasses the developmental cue that enhances plasmodesmata formation between
449 mesophyll and bundle sheath cells is not known. However, *Setaria viridis* and maize show
450 some plasticity in plasmodesmal density in response to growth irradiance (Danila et al.,
451 2019). Our data has further emphasized an important role for light and photosynthesis in
452 establishing plasmodesmal frequency by showing that light rapidly triggers the formation of
453 plasmodesmata at the mesophyll-bundle sheath interface in *G. gynandra*.

454 Plasmodesmata are either formed *de novo* during cell division by trapping ER strands
455 between enlarging Golgi-derived vesicles in new cell walls (primary plasmodesmata) or
456 formed into pre-existing cell walls (secondary plasmodesmata) (Hepler, 1982; Ehlers and
457 Kollmann, 2001; Faulkner et al., 2008). We believe that the increase in plasmodesmata
458 numbers between mesophyll and bundle sheath cell during dark to light transition is driven
459 by the formation of secondary plasmodesmata. Firstly, cotyledon growth from dark to light

460 is thought to be exclusively driven by cell expansion and not cell division in Arabidopsis
461 (Tsukaya et al., 1994; Stoyanova-Bakalova et al., 2004). Secondly, the basic structure of
462 bundle sheath cells was already formed in dark grown seedlings, and the formation of
463 plasmodesmata was rapid. Our SEM mapping technique provided sufficient resolution to
464 observe branching in plasmodesmata (Fig. 2,4-6), but interestingly we did not observe any
465 structural differences between the plasmodesmata in different cell interfaces. Although
466 primary and secondary plasmodesmata can be sometimes distinguished by structure, where
467 secondary plasmodesmata are more branched, this is highly dependent on other factors
468 such as leaf age and sink-source transition (Roberts et al., 2001).

469

470 **A role for metabolism and organelles in formation of plasmodesmata**

471 Our results suggest that chloroplasts, and more specifically photosynthesis, fuel the
472 formation of secondary plasmodesmata between mesophyll and bundle sheath cells in *C₄*
473 *G. gynandra*. Inhibition of photosynthesis and chloroplast development through the
474 application of chemical inhibitors greatly reduced plasmodesmata formation during
475 deetiolation but this effect could be rescued by the exogenous supply of sucrose (Fig. 5,6).
476 Although to our knowledge, a role of photosynthate in controlling formation of
477 plasmodesmata has not been proposed previously some findings are consistent with this
478 hypothesis. For example, in rice constitutive overexpression of the *C₄* maize *GOLDEN2-*
479 *LIKE* transcription that controls chloroplast biogenesis (Waters et al., 2008) not only
480 activated chloroplast and mitochondria development in bundle sheath cells but also
481 increased plasmodesmata numbers between the mesophyll and bundle sheath as well as
482 the bundle and mestome sheath (Wang et al., 2017). Moreover, in *A. thaliana* links between
483 organelles and plasmodesmata have been reported. *A. thaliana* mutants with altered cell-
484 to-cell connectivity and/or plasmodesmata structure such INCREASED SIZE EXCLUSION
485 LIMIT1 and 2 (ISE1/ISE2) encode mitochondrial and chloroplast RNA helicases respectively
486 (Kobayashi et al., 2007; Stonebloom et al., 2009), while the GFP ARRESTED
487 TRAFFICKING1 (GAT1) locus encodes a chloroplast thioredoxin (Benitez-Alfonso et al.,
488 2009). However, the mechanisms of how these organelle-localized proteins affect
489 plasmodesmata formation are poorly understood. Retrograde signaling from chloroplast to
490 nucleus has also been proposed to control plasmodesmata formation and regulation (Burch-
491 Smith et al., 2011; Ganusova et al., 2020). The fact that exogenous supply of sucrose is
492 sufficient to sustain plasmodesmata formation in the presence of DCMU (Fig. 6) strongly
493 suggests a direct metabolic role of chloroplasts in plasmodesmata formation. This may
494 involve sucrose/photosynthesis providing energy required for plasmodesmata formation, or

495 sucrose acting as a signalling molecule to trigger plasmodesmata formation via sugar
496 signalling, and further work will be required to address how sugar controls plasmodesmata
497 formation in *G. gynandra*. However, our work demonstrates that increased plasmodesmal
498 connectivity is likely conserved trait found in both C₄ dicotyledons and monocotyledons.
499 Moreover, the enhanced formation of plasmodesmata between mesophyll and bundle
500 sheath cells of C₄ leaves is co-ordinated and dependent on photosynthesis. Evolution
501 therefore appears to have wired the enhanced formation of plasmodesmata in C₄ leaves to
502 the development of chloroplasts and ultimately the induction of photosynthesis.

503 **DATA AVAILABILITY**

504 The data supporting the findings of this study are available from the corresponding author
505 upon request.

506

507

508 **ACKNOWLEDGEMENTS**

509 The work was funded by the Advanced European Research Council (grant 694733
510 REVOLUTION to J.M.H.). T.B.S. was supported by the Swiss National Science Foundation
511 (SNSF) Early Postdoc Mobility Fellowship (P2EZIP3_181620), the SNSF Postdoc Mobility
512 Fellowship (P500PB_203128) and the EMBO Long-Term Fellowship (ALTF 531-2019). C.F.
513 was funded by the European Research Council (grant 725459 INTERCELLAR to C.F.) and
514 Biotechnology and Biological Research Council Institute Strategic Programme (Plant
515 Health, BBS/E/J/000PR9796 to the John Innes Centre.). For the purpose of open access
516 the authors have applied a Creative Commons Attribution (CC BY) licence to any Author
517 Accepted Manuscript version arising from this submission. We thank Filomena Gallo and
518 Lyn Carter from the Cambridge Advanced Imaging Centre for the electron microscopy
519 sample preparation as well as the support during the image acquisition. We thank Miriam
520 Lucas from Scope M at ETH Zurich for advice and assistance with SBF-SEM. We also thank
521 for Zhengao Di for help with the chlorophyll fluorescence measurement settings.

522

523

524 **CONFLICT OF INTEREST**

525 We have no conflicts of interests to declare.

526

527

528 **AUTHOR CONTRIBUTIONS**

529 T.B.S. and J.M.H. conceived and directed the research; T.B.S., C.F., S.C.Z. and J.M.H.
530 designed the experiments; T.B.S., K.M. and S.E. performed research and analyzed data;
531 T.B.S. and J.M.H. wrote the article with input from all the authors.

532

533

534

535

536

537

538 **REFERENCES**

539

540 Benitez-Alfonso Y, Cilia M, San Roman A, Thomas C, Maule A, Hearn S, Jackson D. (2009)
541 Control of Arabidopsis meristem development by thioredoxin-dependent regulation of
542 intercellular transport. PNAS 106: 3615–3620

543

544 Botha, CEJ (1992) Plasmodesmatal distribution, structure and frequency in relation to
545 assimilation in C₃ and C₄ grasses in southern Africa. Planta 187: 348–358.

546

547 Botha CEJ, Hartley BJ, Cross RHM (1993). The Ultrastructure and Computer-enhanced
548 Digital Image Analysis of Plasmodesmata at the Kranz Mesophyll-Bundle Sheath Interface
549 of *Themeda triandra* var. *imberbis* (Retz) A. Camus in Conventionally-fixed Leaf Blades.
550 Annals of Botany, 72(3):255-261.

551

552 Bowes G, Ogren WL and Hageman RH (1971) Phosphoglycolate production catalyzed by
553 ribulose diphosphate carboxylase. Biochemical and Biophysical Research Communications
554 45:716–722.

555

556 Bräutigam A, Kajala K, Wullenweber J, Sommer M, Gagneul D, Weber KL, Carr KM, Gowik
557 U, Mass J, Lercher MJ, Westhoff P, Hibberd JM and Weber AP (2011) An mRNA blueprint
558 for C₄ photosynthesis derived from comparative transcriptomics of closely related C₃ and C₄
559 species. Plant Physiology 155(1):142-56.

560

561 Brown NJ, Parsley K and Hibberd JM (2005) The futured C₄ research– maize, Flaveria or
562 Cleome? Trends in Plant Science 10:215-221.

563

564 Burch-Smith TM, Brunkard JO, Choi YG, Zambryski PC. (2011) Organelle-nucleus cross-
565 talk regulates plant intercellular communication via plasmodesmata. Proc. Natl Acad. Sci.
566 USA 108, E1451-E1460. doi:10.1073/pnas.1117226108

567

568 Burgess SJ, Granero-Moya I, Grangé-Guermente MJ, Bournsnell C, Terry MJ and Hibberd
569 JM (2016) Ancestral light and chloroplast regulation form the foundations for C₄ gene
570 expression. Nature Plants 16161(2) DOI: 10.1038/NPLANTS.2016.161

571

- 572 Burgess SJ and Hibberd JM (2015) Insights into C₄ metabolism from comparative deep
573 sequencing. *Current Opinion of Plant Biology* 25:138-144.
574
- 575 Cackett L, Luginbühl LH, Schreier TB, Lopez-Juez E and Hibberd JM (2021) Chloroplast
576 development in green plant tissues: the interplay between light, hormone, and transcriptional
577 regulation. *New Phytologist* 233(5): 2000-2016.
578
- 579 Chamovitz D, Pecker I, Hirschberg J. (1991) The molecular basis of resistance to the
580 herbicide norflurazon. *Plant Mol Biol.* 16(6):967-74. doi: 10.1007/BF00016069. PMID:
581 1907510.
582
- 583 Danila FR, Quick WP, White RG, Furbank RT and von Caemmerer S (2016) The metabolite
584 pathway between bundle sheath and mesophyll: Quantification of plasmodesmata in leaves
585 of C₃ and C₄ monocots. *Plant Cell* 6:1461-71.
586
- 587 Danila FR, Quick WP, White RG, White RG, Kelly S, von Caemmerer S and Furbank RT
588 (2018) Multiple mechanisms for enhanced plasmodesmata density in disparate subtypes of
589 C₄ grasses. *J Exp Bot* <https://doi.org/10.1093/jxb/erx456>
590
- 591 Danila FR, Quick WP, White RG, von Caemmerer S and Furbank RT (2019) Response of
592 plasmodesmata formation in leaves of C₄ grasses to growth irradiance. *Plant, Cell &*
593 *Environment* 42 (8):2482-2494.
594
- 595 Deinum EE, Mulder BM, Benitez-Alfonso Y (2019). From plasmodesma geometry to
596 effective symplasmic permeability through biophysical modelling. *Elife.* 8:e49000.
597
- 598 Ehlers K, Kollmann R (2001) Primary and secondary plasmodesmata: structure, origin, and
599 functioning. *Protoplasma* 216:1–30.
600
- 601 Evert RF, Eschrich W and Heyser W (1977) Distribution and structure of plasmodesmata in
602 mesophyll and bundle-sheath cells of *Zea-mays-L.* *Planta*, 136:77-89.
603
- 604 Faulkner C (2018). Plasmodesmata and the symplast, *Current Biology* 28(24):1374-1378.
605 <https://doi.org/10.1016/j.cub.2018.11.004>
606

- 607 Faulkner C, Akman OE, Bell K, Jeffree C, Oparka K (2008) Peeking into pit fields: a multiple
608 twinning model of secondary plasmodesmata formation in tobacco. *Plant Cell*. 20(6):1504-
609 18. doi: 10.1105/tpc.107.056903.
- 610
- 611 Ganusova EE, Reagan BC, Fernandez JC, Azim MF, Sankoh AF, Freeman KM, McCray
612 TN, Patterson K, Kim C, Burch-Smith TM. (2020) Chloroplast-to-nucleus retrograde
613 signalling controls intercellular trafficking via plasmodesmata formation. *Philos Trans R Soc
614 Lond B Biol Sci*. 375(1801):20190408. doi: 10.1098/rstb.2019.0408.
- 615
- 616 Guseman JM, Lee JS, Bogenschutz NL, Peterson KM, Virata RE, et al. (2010) Dysregulation
617 of cell-to-cell connectivity and stomatal patterning by loss-of-function mutation in
618 *Arabidopsis* CHORUS (GLUCAN SYNTHASELIKE 8). *Development* 137: 1731–1741.
- 619
- 620 Hatch MD (1987). C₄ photosynthesis: a unique blend of modified biochemistry, anatomy and
621 ultrastructure. *Biochim. Biophys. Acta* 895: 81–106.
- 622
- 623 Hatch M D and Osmond CB (1976). In *Transport in Plants III Encyclopedia of Plant
624 Physiology Vol. 3* (eds Stocking, C. R. & Heber, U.) Ch. 5, 144–184 (Springer, 1976).
- 625
- 626 Hepler PK. (1982) Endoplasmic reticulum in the formation of the cell plate and
627 plasmodesmata. *Protoplasma* 111:121–133.
- 628
- 629 Hughes A, Faulkner C, Morris RJ and Tomkins M (2021). Intercellular Communication as a
630 Series of Narrow Escape Problems, *IEEE Transactions on Molecular, Biological and Multi-
631 Scale Communications*, 7(2):89-93. doi: 10.1109/TMBMC.2021.3083719.
- 632
- 633 Kobayashi K, Otegui MS, Krishnakumar S, Mindrinos M, and Zambryski P (2007)
634 INCREASED SIZE EXCLUSION LIMIT 2 encodes a putative DEVH box RNA helicase
635 involved in plasmodesmata function during *Arabidopsis* embryogenesis. *Plant Cell* 19:1885-
636 1897.
- 637
- 638 Koteyeva NK, Voznesenskaya EV, Roalson EH, Edwards GE (2011) Diversity in forms of
639 C₄ in the genus *Cleome* (*Cleomaceae*), *Annals of Botany* 107(2):269–283.
640 <https://doi.org/10.1093/aob/mcq239>
- 641

- 642 Koteyeva NK, Voznesenskaya EV, Cousins AB, Edwards GE (2014) Differentiation of C₄
643 photosynthesis along a leaf developmental gradient in two Cleome species having different
644 forms of Kranz anatomy. J Exp Bot, 65(13):3525–3541. <https://doi.org/10.1093/jxb/eru042>
645
- 646 Leegood RC (2002) C₄ photosynthesis: principles of CO₂ concentration and prospects for
647 its introduction into C₃ plants. Journal of Experimental Botany 53 (369):581–590.
648
- 649 Marshall DM, Muhaidat R, Brown NJ, Liu Z, Stanley S, Griffiths H, Sage RF, Hibberd JM
650 (2007) Cleome, a genus closely related to Arabidopsis, contains species spanning a
651 developmental progression from C₃ to C₄ photosynthesis. The Plant Journal 55:886-896.
652 doi: 10.1111/j.1365-313X.2007.03188.x
653
- 654 Mulo P, Pursiheimo S, Hou CX, Tyystjärvi T, Aro EM (2003) Multiple effects of antibiotics on
655 chloroplast and nuclear gene expression. Funct Plant Biol. 30(11):1097-1103. doi:
656 10.1071/FP03149. PMID: 32689092.
657
- 658 Newell CA, Brown NJ, Liu Z, Pflug A, Gowik U, Westhoff P, and Hibberd JM (2010)
659 Agrobacterium tumefaciens-mediated transformation of Cleome gynandra L., a C₄
660 dicotyledon that is closely related to Arabidopsis thaliana. J Exp Bot 61(5):1311-1319.
661
- 662 Nicolas WJ, Grison MS, Trépout S, Gaston A, Fouché M, Cordelières FP, Oparka K, Tilsner
663 J, Brocard L and Bayer EM (2017) Architecture and permeability of post-cytokinesis
664 plasmodesmata lacking cytoplasmic sleeves. Nature plants 3:17082.
665
- 666 Radford JE, Vesik M, Overall RL (1997) Callose deposition at plasmodesmata. Protoplasma
667 201: 30–37.
668
- 669 Paterlini A, Belevich I (2022) Serial Block Electron Microscopy to Study Plasmodesmata
670 in the Vasculature of Arabidopsis thaliana Roots. Yoselin Benitez-Alfonso and Manfred
671 Heinlein (eds.), Plasmodesmata: Methods and Protocols, Methods in Molecular Biology, vol.
672 2457, https://doi.org/10.1007/978-1-0716-2132-5_5
673
- 674 Pipitone R, Eicke S, Pfister B, Glauser G, Falconet D, Uwizeye C, Pralon T, Zeeman SC,
675 Kessler F, Demarsy E (2021) A multifaceted analysis reveals two distinct phases of
676 chloroplast biogenesis during de-etiolation in Arabidopsis eLife 10:e62709.

677

678 Reeves G, Singh P, Rossber TA, Sogbohossou D, Schranz E, and Hibberd JM (2018)
679 Quantitative variation within a species for traits underpinning C₄ photosynthesis. *Plant*
680 *Physiology*, Volume 177, Issue 2, June 2018, Pages 504–512,
681 <https://doi.org/10.1104/pp.18.00168>

682

683 Roberts IM, Boevink P, Roberts AG, Sauer N, Reichel C, Oparka KJ. (2001) Dynamic
684 changes in the frequency and architecture of plasmodesmata during the sink-source
685 transition in tobacco leaves. *Protoplasma*. 218(1-2):31-44. doi: 10.1007/BF01288358.

686

687 Ross-Elliott T, Jensen KH, Haaning KS, Wager BM, Knoblauch J, Howell AH, Mullendore
688 DL, Monteith AG, Paultre D, Yan D, Otero S, Bourdon M, Sager R, Lee JY, Helariutta Y,
689 Knoblauch M, and Oparka KJ (2017) Phloem unloading in *Arabidopsis* roots is convective
690 and regulated by the phloem-pole pericycle. *eLife* 6:e24125.

691

692 Sage RF, Christin PA and Edwards EJ (2011) The C₄ plant lineages of planet Earth. *J Exp*
693 *Bot* 62: 3155–3169.

694

695 Shen Z, Li P, Ni RJ, Ritchie M, Yang CP, Liu GF, Ma W, Liu GJ, Ma L, Li SJ, Wei ZG, Wang
696 HX, Wang BC (2009) Label-free quantitative proteomics analysis of etiolated maize seedling
697 leaves during greening. *Mol Cell Proteomics*. 8(11):2443-60. doi: 10.1074/mcp.M900187-
698 MCP200.

699

700 Simpson C, Thomas C, Findlay K, Bayer E, Maule AJ (2009) An *Arabidopsis* GPI-Anchor
701 Plasmodesmal Neck Protein with Callose Binding Activity and Potential to Regulate Cell-to-
702 Cell Trafficking. *Plant Cell* 21: 581–594.

703

704 Singh P, Stevenson SR, Reeves G, Schreier TB and Hibberd JM (2021) Induction of C₄
705 genes evolved through changes in cis allowing integration into ancestral C₃ gene regulatory
706 networks. *bioRxiv* <https://doi.org/10.1101/2020.07.03.186395>

707

708 Stonebloom S, Burch-Smith T, Kim I, Meinke D, Mindrinos M, and Zambryski P (2009) Loss
709 of the plant DEADbox protein ISE1 leads to defective mitochondria and increased cell-to-
710 cell transport via plasmodesmata. *PNAS* 106(40):17229-17234.

711

712 Stoyanova-Bakalova, E., Karanov, E., Petrov, P. and Hall, M.A. (2004), Cell division and cell
713 expansion in cotyledons of Arabidopsis seedlings. *New Phytologist*, 162: 471-479.
714 <https://doi.org/10.1111/j.1469-8137.2004.01031.x>

715

716 Trebst, A. (2007). Inhibitors in the functional dissection of the photosynthetic electron
717 transport system. *Photosynth Res.* 92, 217–224. doi: 10.1007/s11120-007-9213-x

718

719 Tsukaya H, Tsuge T, Uchimiya T. (1994). The cotyledon: a superior system for studies of
720 leaf development. *Planta* 195: 309–312.

721

722 Von Caemmerer S. (2021). Updating the steady-state model of C₄ photosynthesis. *J Exp*
723 *Bot.* 72(17):6003-6017. doi: 10.1093/jxb/erab266.

724

725 Wang P, Khoshravesh R, Karki S, Tapia R, Balahadia CP, Bandyopadhyay A, Quick WP,
726 Furbank R, Sage TL, Langdale JA. (2017) Re-creation of a Key Step in the Evolutionary
727 Switch from C₃ to C₄ Leaf Anatomy. *Curr Biol.* 27(21):3278-3287.e6. doi:
728 10.1016/j.cub.2017.09.040.

729

730 Wang Y, Stutz SS, Bernacchi CJ, Boyd RA, Ort DR, Long SP (2022). Increased bundle-
731 sheath leakiness of CO₂ during photosynthetic induction shows a lack of coordination
732 between the C₄ and C₃ cycles. *New Phytologist*. doi: 10.1111/nph.18485.

733

734 Waters MT, Moylan EC, Langdale JA (2008) GLK transcription factors regulate chloroplast
735 development in a cell-autonomous manner. *The Plant Journal* 56, 432–444. doi:
736 10.1111/j.1365-313X.2008.03616.x.

737

738

739 **SUPPORTING INFORMATION**

740

741 **Supporting Information Videos 1. Compiled video of sequential 50 nm sections of M-**
742 **BS cell interface in mature leaves of C₄ *G. gynandra*.**

743

744 **Supporting Information Videos 2. Compiled video of sequential 50 nm sections of M-**
745 **BS cell interface in mature leaves of C₃ *T. hassleriana*.**

746

747 **Supporting Information Videos 3. Compiled video of sequential 50 nm sections of M-**
748 **BS cell interface in mature leaves of C₃ *A. thaliana*.**

749

750 **Supporting Information Figure 1. Transmission electron micrographs of M-BS, M-M**
751 **and BS-BS cell interfaces.**

752

753 **Supporting Information Figure 2. Comparison of plasmodesmal frequencies**
754 **quantified using 2D SEM and 3D SBF-SEM.**

755

756 **Supporting Information Figure 3. Pitfield area is not increased in C₄ *G. gynandra***
757 **compared to C₃ *A. thaliana* and *T. hassleriana*.**

758

759 **Supporting Information Figure 4. Extended dark treatment for 48 h does not increase**
760 **plasmodesmata frequency in *G. gynandra* cotyledons.**

761

762 **Supporting Information 5. Chloroplast inhibitors have limited effect on light-induced**
763 **cotyledon expansion, but affect plasmodesmata formation.**

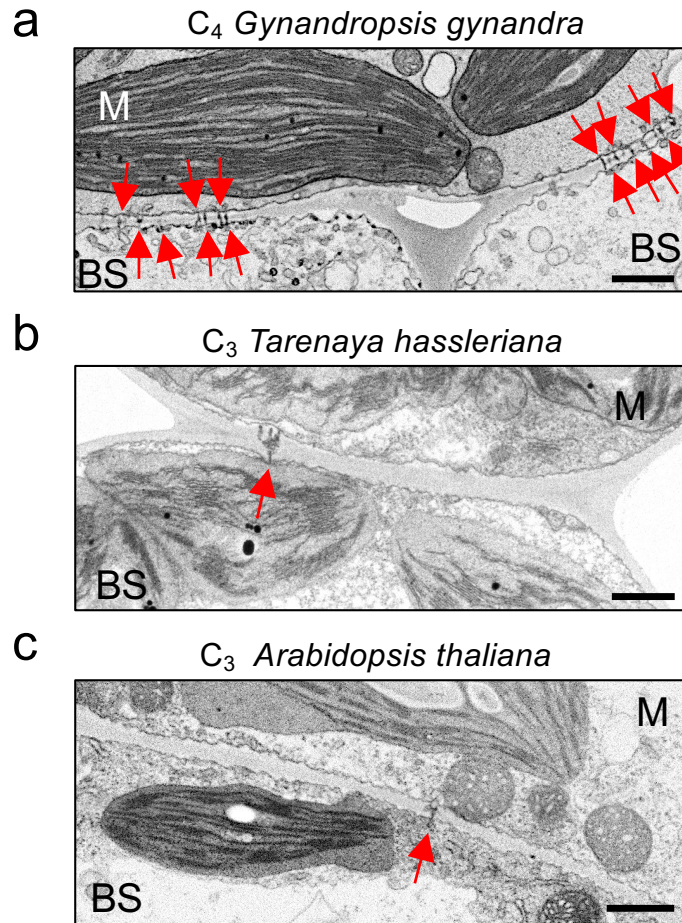
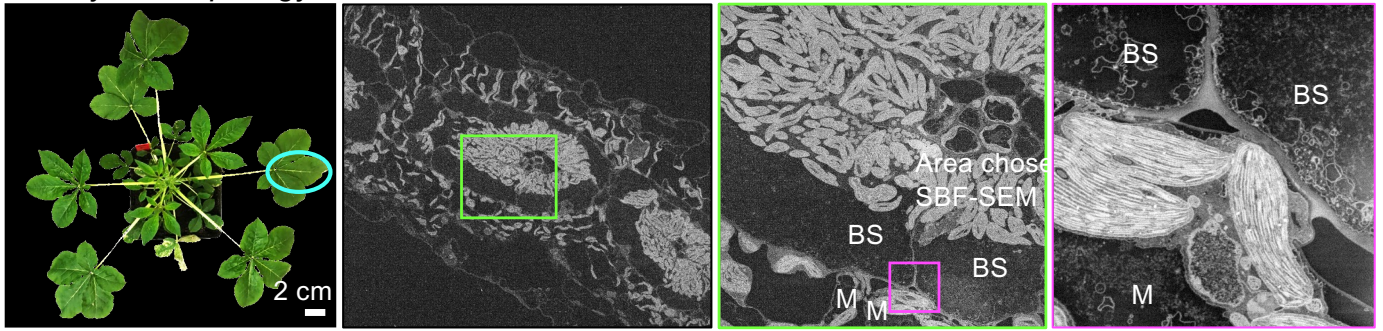
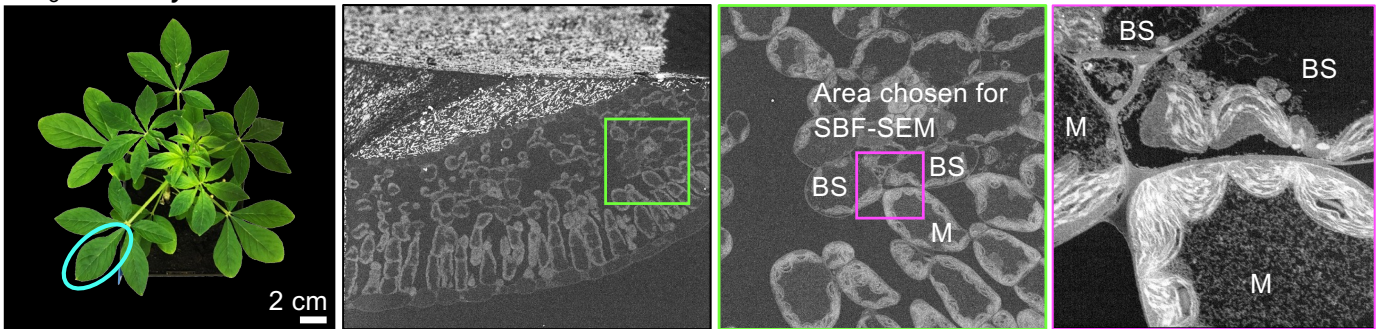


Figure 1. The M-BS cell interface of *C4 Gynandropsis gynandra* has an increased plasmodesmal connections in comparison to the closely related *C3* species. Representative transmission electron micrographs of M-BS interfaces in (a) *C4 G. gynandra*, (b) *C3 T. hassleriana* and (c) *C3 A. thaliana* leaves. Mature leaves were harvested from 4-week-old *G. gynandra* and *T. hassleriana*, and from 3-week-old *A. thaliana* plants. Red arrows indicate individual plasmodesma. Scale bar = 1 μm

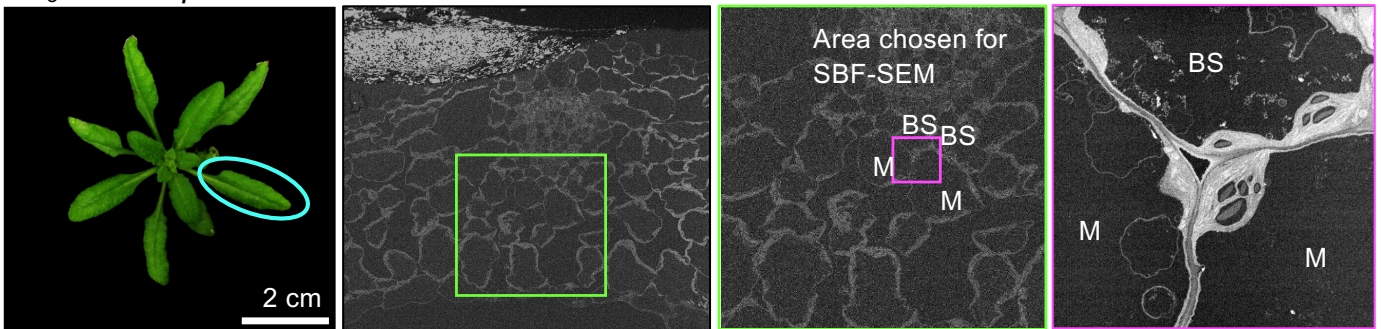
a C_4 *Gynandropsis gynandra*



b C_3 *Tarenaya hassleriana*



c C_3 *Arabidopsis thaliana*



d

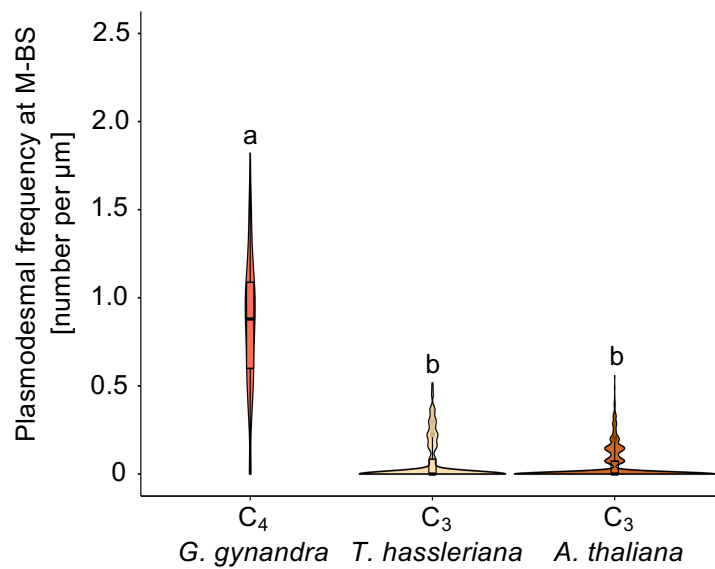


Figure 2. 3D Serial Block Face-SEM (SBF-SEM) analysis of plasmodesmata number at the M-BS cell interface. Left panels: Photographs of 4-week-old (a) *C₄ G. gynandra* and (b) *C₃ T. hassleriana*, and 3-week-old (c) *C₃ A. thaliana* plants. Mature leaves harvested for plasmodesmata quantification are circled. Mid left panels: Scanning electron micrographs of leaf cross sections from (a) *C₄ G. gynandra*, (b) *C₃ T. hassleriana* and (c) *C₃ A. thaliana*. Mid right panels: Zoomed image of the region marked by a green box, showing M-BS cell interface area chosen for SBF-SEM analysis (magenta). Left panels: Single frame of compiled SBF-SEM data into Supporting Information Videos 1-3 of (a) *C₄ G. gynandra* (b) *C₃ T. hassleriana* and (c) *C₃ A. thaliana*. (d) Violin plot of plasmodesmal frequencies measured at M-BS cell interfaces in the three plant species using 3D SBF-SEM data. As some sections contained more than one M-BS cell interface, plasmodesmata frequencies were quantified in total of 476 individual M-BS cell interfaces for *G. gynandra*, 367 individual M-BS cell interfaces for *T. hassleriana* and 886 individual M-BS cell interfaces for *A. thaliana*. The box and whiskers represent the 25 to 75 percentile and minimum-maximum distributions of the data. Letters show the statistical ranking using a *post hoc* Tukey test (different letters indicate significant differences at $P < 0.05$). Values indicated by the same letter are not statistically different.

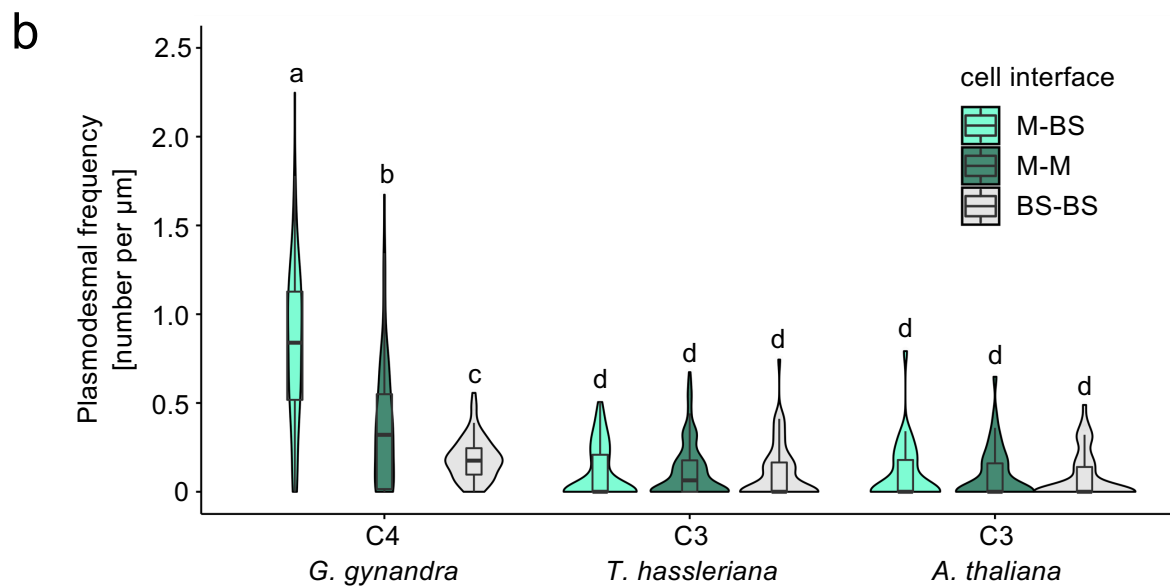
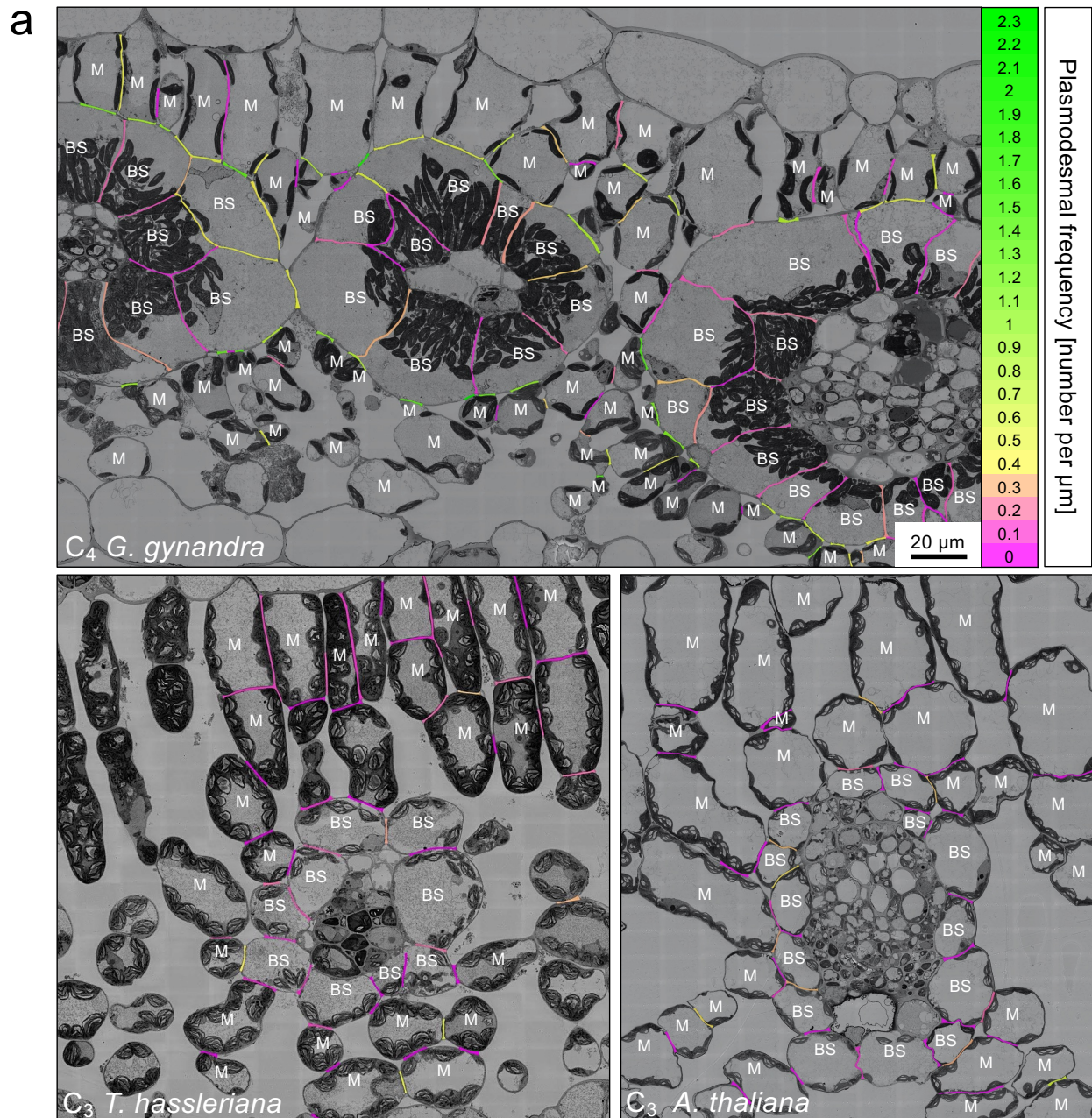


Figure 3. Plasmodesmata frequency in C4 *G. gynandra* is higher at the M-BS interface compared to other interfaces. (a) Plasmodesmata distribution heatmap. Cell interfaces in high-resolution 2D SEM maps of C₄ *G. gynandra*, C₃ *T. hassleriana* and C₃ *A. thaliana* leaf cross sections were coloured according to plasmodesmal frequency (number of plasmodesmata observed on the interface, divided by the interface length [μm]). (b) Plasmodesmal frequency for M-BS, M-M, and BS-BS interfaces in *G. gynandra*, *T. hassleriana* and *A. thaliana* mature leaves, quantified using high-resolution 2D SEM maps. For *G. gynandra*, $n = 86$ M-M, $n = 96$ M-BS and $n = 70$ BS-BS cell interfaces were quantified. For *T. hassleriana*, $n = 202$ M-M, $n = 80$ M-BS and $n = 77$ BS-BS individual cell interfaces were quantified. For *A. thaliana*, $n = 45$ M-M, $n = 37$ M-BS and $n = 54$ BS-BS cell interfaces were quantified. All interfaces were quantified from leaf samples of at least 3 individual plants (biological replicates) per species. The box and whiskers represent the 25 to 75 percentile and minimum-maximum distributions of the data. Letters show the statistical ranking using a *post hoc* Tukey test (different letters indicate significant differences at $P < 0.05$). Values indicated by the same letter are not statistically different.

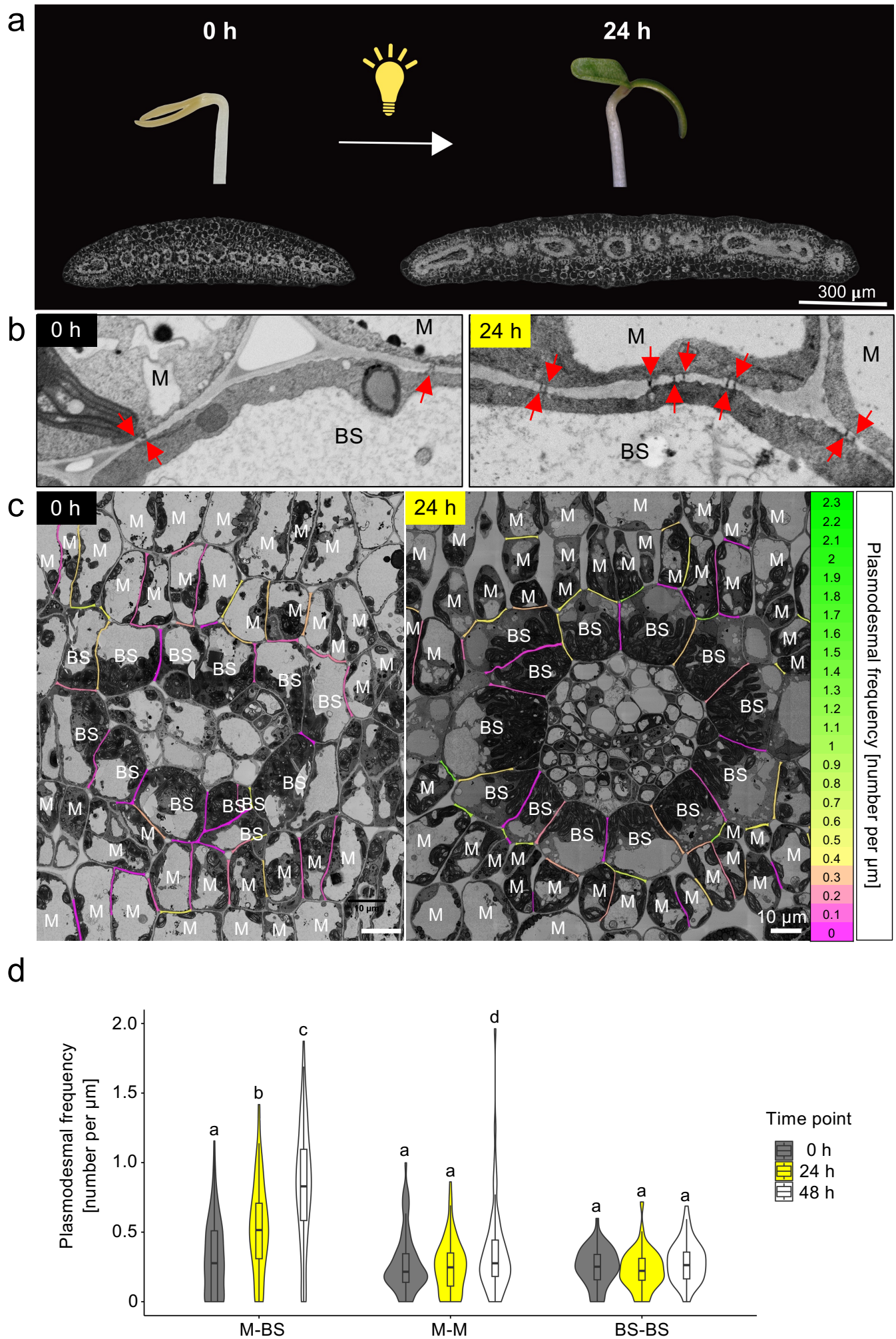


Figure 4. Light acts as a developmental cue for increased plasmodesmata formation at the M-BS cell interface in *C₄ G. gynandra* cotyledons. (a) Photographs of representative etiolated (left) and deetiolated (right) *G. gynandra* seedlings and scanning electron micrographs of cotyledon cross sections at 0 h and 24 h time point. (b) Representative scanning electron micrographs of M-BS interfaces in *C₄ G. gynandra* cotyledons. Red arrows indicate individual plasmodesma. Scale bar = 1 μm (c) Plasmodesmata distribution heatmap. Cell interfaces in high-resolution 2D-SEM maps of *C₄ G. gynandra* cotyledon cross sections, harvested prior to light induction (0 h time point) and after light induction (24 h time point) were coloured according to plasmodesmal frequency (number of plasmodesmata observed on the interface, divided by the interface length [μm]). (d) Plasmodesmata frequency per μm cell interfaces (M-BS, M-M, BS-BS) in *G. gynandra* cotyledons was quantified during dark to light transition (0 h, 24 h and 48 h time point) using high resolution 2D SEM maps. For the 0 h time point, $n = 81$ (M-BS), $n = 74$ (M-M) and $n = 49$ (BS-BS) cell interfaces were quantified. For the 24 h time point, $n = 69$ (M-BS), $n = 70$ (M-M) and $n = 42$ (BS-BS) cell interfaces were quantified. For the 48h time point, $n = 90$ (M-BS), $n = 60$ (M-M) and $n = 49$ (BS-BS) cell interfaces were quantified. All interfaces were quantified from cotyledon samples of at least 3 individual seedlings (biological replicates) per time point. The box and whiskers represent the 25 to 75 percentile and minimum-maximum distributions of the data. Letters show the statistical ranking using a one-way ANOVA with a *post hoc* Tukey test (different letters indicate significant differences at $P < 0.05$). Values indicated by the same letter are not statistically different.

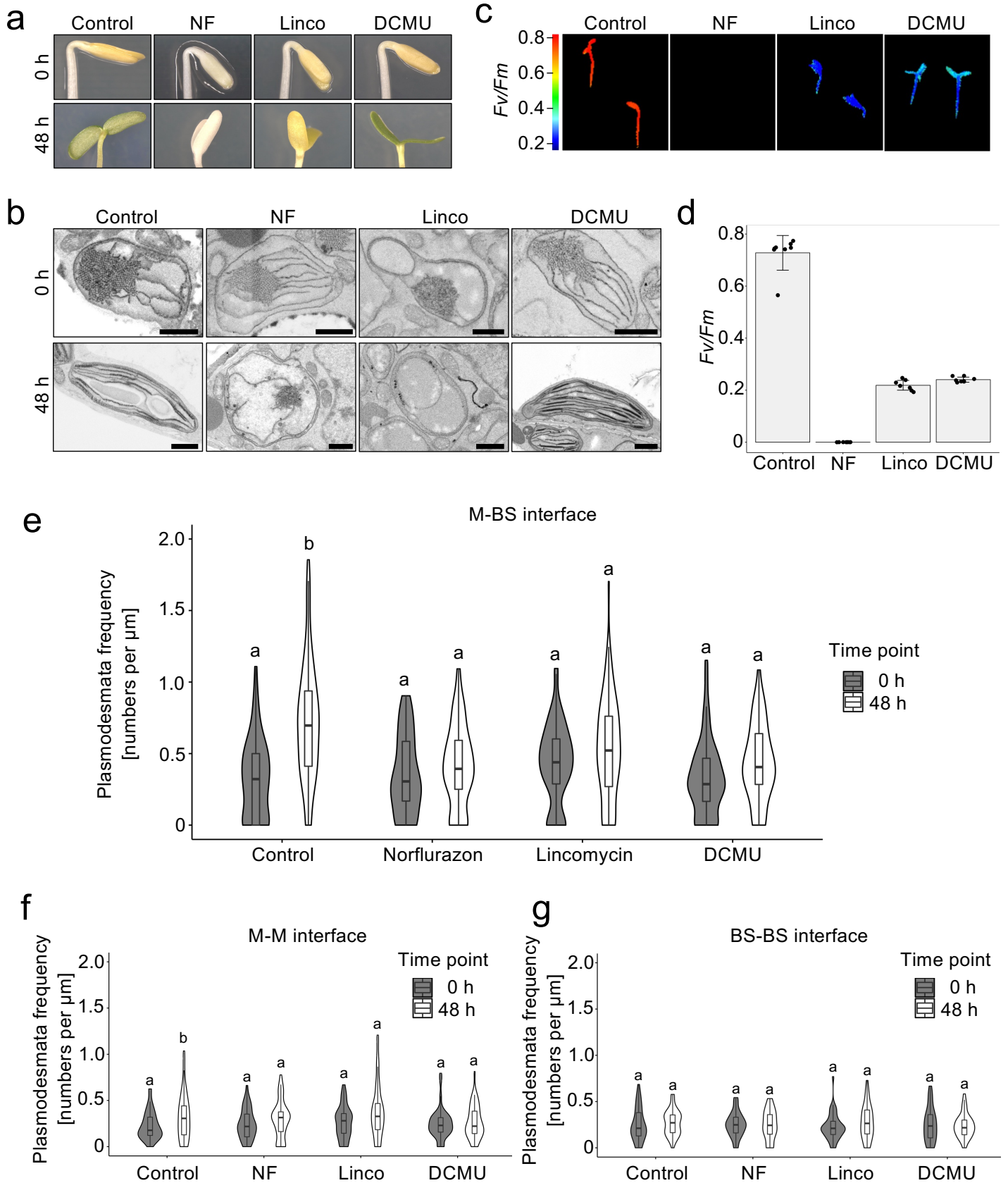


Figure 5. Chloroplast inhibitors significantly reduced plasmodesmata formation at the M-BS interface. The effect of norflurazon (NF), lincomycin (Linco), and DCMU were tested. **(a)** Photographs of *G. gynandra* seedlings treated with inhibitors during deetiolation at 0 h and 48 h. **(b)** Scanning electron micrographs of etioplasts (0 h) and mature chloroplasts (48 h) in inhibitor-treated and untreated (Control) *G. gynandra* seedlings. Scale bar = 1 μm **(c)** Chlorophyll fluorescence images of maximum quantum efficiency of PSII photochemistry (F_v/F_m) from 48 h deetiolated *G. gynandra* seedlings treated with NF, Linco and DCMU, as well as untreated seedlings (Control). **(d)** F_v/F_m measured in inhibitor-treated and untreated *G. gynandra* seedlings at 48 h after light induction. Bars represent mean \pm standard deviation from $n = 7-8$ individual seedlings, dots represent individual data points. **(e-g)** Plasmodesmata frequency per μm cell interfaces in *G. gynandra* cotyledons was quantified during dark to light transition (0 h and 48 h time point) for each individual inhibitor treatment using high-resolution 2D SEM maps: **(e)** M-BS, **(f)** M-M and **(g)** BS-BS. **(e)** For M-BS interface: 0h control $n = 59$, 0h norflurazon $n = 53$, 0h lincomycin $n = 55$, 0h DCMU $n = 50$, 48h control $n = 85$, 48h norflurazon $n = 66$, 48h lincomycin $n = 90$, 48h DCMU $n = 50$ cell interfaces were quantified. **(f)** For M-M interface: 0h control $n = 41$, 0h norflurazon $n = 43$, 0h lincomycin $n = 45$, 0h DCMU $n = 41$, 48h control $n = 45$, 48h norflurazon $n = 45$, 48h lincomycin $n = 45$, 48h DCMU $n = 45$ cell interfaces were quantified. **(g)** For BS-BS interface: 0h control $n = 41$, 0h norflurazon $n = 39$, 0h lincomycin $n = 44$, 0h DCMU $n = 38$, 48h control $n = 45$, 48h norflurazon $n = 45$, 48h lincomycin $n = 43$, 48h DCMU $n = 45$ cell interfaces were quantified. All interfaces were quantified from cotyledon samples of at least 3 individual seedlings (biological replicates) per time point. The box and whiskers represent the 25 to 75 percentile and minimum-maximum distributions of the data. Letters show the statistical ranking, pairwise comparison of 0h and 48 h time point for each treatment, using a *post hoc* Tukey test (different letters indicate significant differences at $P < 0.05$). Values indicated by the same letter are not statistically different.

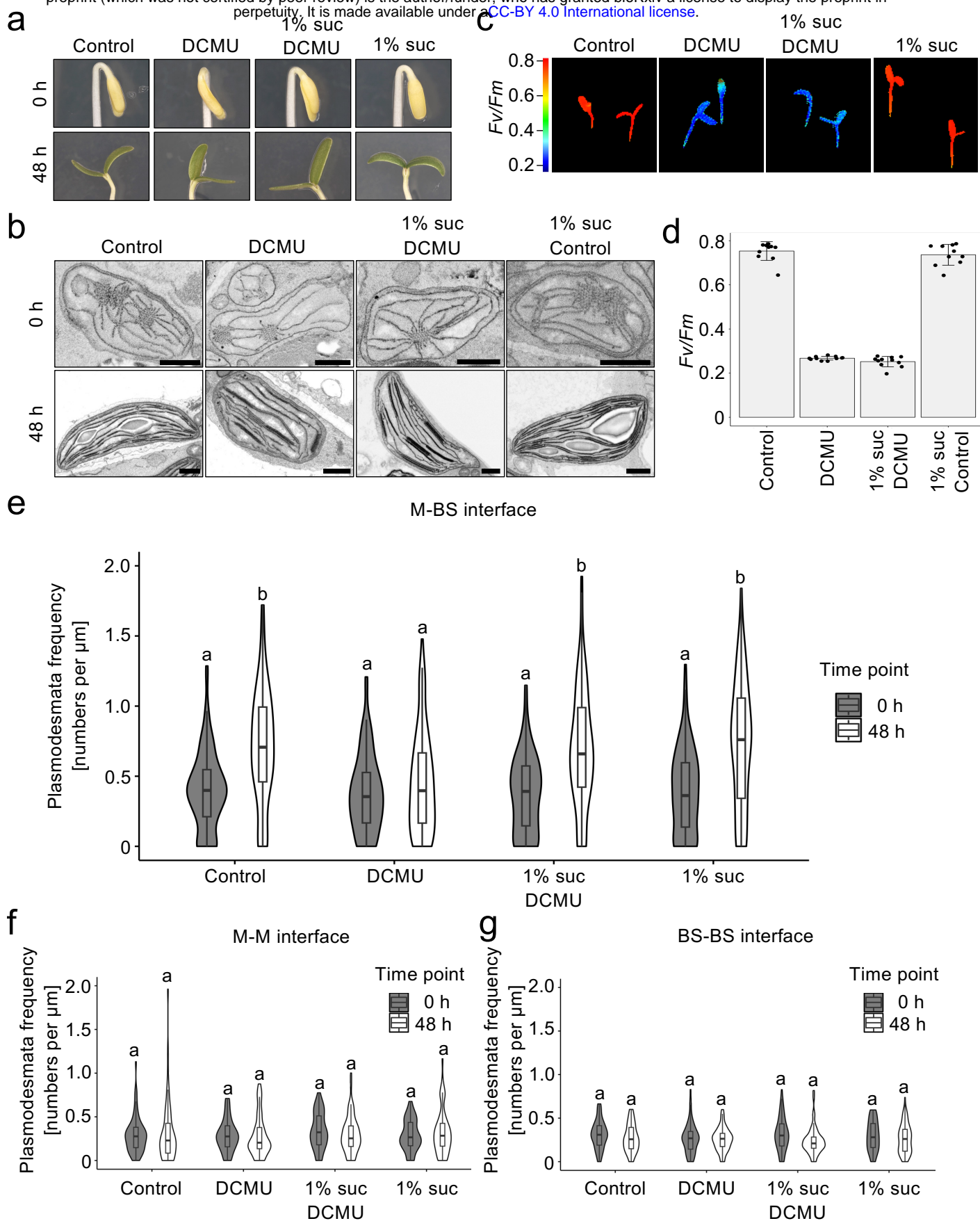


Figure 6. DCMU-inhibited plasmodesmata formation at the M-BS interface could be rescued by sucrose. (a) Photographs of DCMU-treated *G. gynandra* seedlings during deetiolation (at 0 h and 48 h) with or without exogenous 1% sucrose. (b) Scanning electron micrographs of etioplasts (0 h) and mature chloroplasts (48 h) of DCMU-treated and untreated (Control) *G. gynandra* seedlings with or without exogenous 1% sucrose. Scale bar = 1 μm (c) Chlorophyll fluorescence images of maximum quantum efficiency of PSII photochemistry (F_v/F_m) from 48 h deetiolated *G. gynandra*, untreated and DCMU-treated. (d) F_v/F_m measured in *G. gynandra* 48 h after light induction. Bars represent mean \pm standard deviation from $n = 7-8$ individual seedlings, dots represent individual data points. (e-g) Plasmodesmata frequency per μm cell interfaces in *G. gynandra* cotyledons was quantified during dark to light transition (0 h and 48 h time point) and DCMU treatment, with and without additional 1% sucrose supply, using high-resolution 2D SEM maps: (e) M-M, (f) M-BS and (g) BS-BS. All interfaces were quantified from cotyledon samples of at least 3 individual seedlings (biological replicates) per time point. (e) For M-BS interface: 0h control_nosuc $n = 96$, 0h DCMU_nosuc $n = 82$, 0h control_suc $n = 84$, 0h DCMU_suc $n = 87$, 48h control_nosuc $n = 79$, 48h DCMU_nosuc $n = 98$, 48h control_suc $n = 101$, 48h DCMU_suc $n = 96$ cell interfaces were quantified. (f) For M-M interface: 0h control_nosuc $n = 64$, 0h DCMU_nosuc $n = 57$, 0h control_suc $n = 65$, 0h DCMU_suc $n = 63$, 48h control_nosuc $n = 55$, 48h DCMU_nosuc $n = 60$, 48h control_suc $n = 58$, 48h DCMU_suc $n = 55$ cell interfaces were quantified. (g) For BS-BS interface: 0h control_nosuc $n = 65$, 0h DCMU_nosuc $n = 62$, 0h control_suc $n = 53$, 0h DCMU_suc $n = 57$, 48h control_nosuc $n = 48$, 48h DCMU_nosuc $n = 53$, 48h control_suc $n = 62$, 48h DCMU_suc $n = 55$ cell interfaces were quantified. The box and whiskers represent the 25 to 75 percentile and minimum-maximum distributions of the data. Letters show the statistical ranking, pairwise comparison of 0h and 48 h time point for each treatment, using a *post hoc* Tukey test (different letters indicate significant differences at $P < 0.05$). Values indicated by the same letter are not statistically different.